SARS-CoV-2 infects human GnRH neurons and tanycytes, disrupting hypothalamic-pituitary hormonal axes

Florent Sauve
Inserm
Sreekala Nampoothiri
Inserm
Daniela Fernandois
Inserm https://orcid.org/0000-0002-8282-0189
Caio Coelho
Inserm
Julie Dam
Institut Cochin Inserm https://orcid.org/0000-0001-6871-2678
Gaëtan Ternier
Inserm
Ludovica Cotellessa
Inserm
Cristina Iglesias
University of Santiago de Compostela
Helge Müller-Fielitz
University of Luebeck https://orcid.org/0000-0003-2815-4426
Julie Dewisme
Inserm
Erika Cecon
Inserm
Thibaud Lebouvier
Inserm UMR-S 1172
Romain Perbet
Univ. Lille, Inserm, CHU Lille, U1172 - LilNCog - Lille Neuroscience & Cognition, F-59000 Lille, France
https://orcid.org/0000-0001-5974-4061
Vincent Florent
Inserm
Marc Baroncini
Inserm U1172

Ariane Sharif
Inserm
June Ereño-Orbea
CIC bioGUNE
Maria Mercado-Gomez
CIC bioGUNE
Asis Palazon
CIC bioGUNE
Virginie Mattot
Inserm
Florence Pasquier
Ctr Hosp Reg & Univ Lille https://orcid.org/0000-0001-9880-9788
Sophie Catteau-Jonard
CHU Lille, Service de Gynécologie Médicale, Hôpital Jeanne de Flandre, Lille
Ralf Jockers
Institut Cochin, Université Paris Descartes, CNRS (UMR 8104), Paris F-75014, France
https://orcid.org/0000-0002-4354-1750
Laurent Storme
CHU Lille
Erik Hrabovszky
Hungarian Academy of Sciences
François Trottein
Pasteur Institute of Lille
María Martínez-Chantar
Liver Disease Lab, CIC bioGUNE, Basque Research and Technology Alliance (BRTA); Centro de Investigación Biomédica en Red de Enfermedades Hepáticas y Digestivas (CIBEhd)
https://orcid.org/0000-0002-6446-9911
Ruben Nogueiras
CIMUS, University of Santiago de Compostela-Instituto de Investigación Sanitaria
https://orcid.org/0000-0002-9976-9930
Markus Schwaninger
University of Lübeck https://orcid.org/0000-0002-4510-9718
Pascal Pigny
Service Hormonologie Métabolisme Nutrition, Centre de biologie pathologie génétique, CHRU Lille
Julien Poissy
Centre Hospitalier Regional et Universitaire de Lille
Konstantina Chachlaki
Inserm
Claude-Alain Maurage

Inserm

Paolo Giacobini

Univ. Lille, Inserm, CHU Lille, U1172 - LilNCog - Lille Neuroscience & Cognition https://orcid.org/0000-0002-3075-1441

S Rasika

Inserm https://orcid.org/0000-0001-8733-4641

Vincent Prevot (vincent.prevot@inserm.fr)

Inserm https://orcid.org/0000-0001-7185-3615

Article

Keywords: SARS-CoV-2, low testosterone levels, gonadotropin-releasing hormone

Posted Date: November 12th, 2021

DOI: https://doi.org/10.21203/rs.3.rs-1050969/v1

Abstract

Neuroinvasion by SARS-CoV-2 is now accepted. To investigate whether low testosterone levels observed in men with severe COVID-19 could be of central origin, we retrospectively analyzed blood samples from 60 male intensive-care patients and explored SARS-CoV-2 brain entry using animal and cellular models as well as adult COVID-19 patient and fetal human brains. Most hypotestosteronemic patients displayed hypogonadotropic hypogonadism or abnormal hypothalamic-pituitary-gonadal axis regulation. Neurons producing gonadotropin-releasing hormone (GnRH), the master molecule controlling fertility, expressed angiotensin-converting enzyme 2 and neuropilin-1, two host-cell factors mediating infection, and were infected and dying in all COVID-19 patient brains. Tanycytes - hypothalamic glia that regulate GnRH secretion - were also infected. Additionally, human fetal olfactory and vomeronasal epithelia, from which GnRH neurons arise, richly expressed both the above host-cell susceptibility factors and formyl peptide receptor 2, a putative vomeronasal receptor that also appeared involved in SARS-CoV-2 pathogenesis in humans and mice. Finally, a fetal human GnRH cell line expressing all these receptors could be infected by a SARS-CoV-2-like pseudovirus. Together, our findings suggest that GnRH neurons, which may be implicated in brain development and aging in addition to reproduction, are particularly vulnerable to SARS-CoV-2 in both adults and fetuses/newborns, with potentially devastating long-term consequences.

Introduction

Two years into the COVID-19 pandemic, it is increasingly evident that few if any tissues of the human body are resistant to infection by SARS-CoV-2. In addition to the respiratory tract, viral RNAs or proteins have been detected in several peripheral organs, and there are now multiple reports of neuroinvasion that could underlie the various neurological symptoms observed in COVID-19 patients. However, the dysfunction of peripheral organs and bodily processes could also stem from brain infection, with potentially worrying long-term consequences. This is particularly true of the hypothalamus, which lies at the crossroads of several putative infection routes, and whose diverse neuroglial populations participate in both hypothalamic-brainstem physiological circuits as well as hypothalamic-pituitary neuroendocrine circuits that regulate a vast range of functions, including reproduction and fertility. Indeed, a number of scientific studies and popular reports have suggested that the virus could interfere with reproductive function [1].

In humans, neurons secreting gonadotropin-releasing hormone (GnRH), the master regulator of the development of the reproductive axis and adult fertility, constitute a sparse population of barely a couple of thousand cells [2], principally located in the infundibular nucleus of the tuberal region of the hypothalamus [2,3]. These neurons send projections to the external zone of the median eminence, where they release the neurohormone in the vicinity of the pituitary portal blood vessels, which are characterized by a “fenestrated” or highly permeable capillary wall instead of the usual tightly sealed endothelial layer that constitutes the blood-brain barrier (BBB). In the external zone of the median eminence, these GnRH neuronal terminals intermingle with and are ensheathed by the glial processes of tanycytes [3], specialized

radial-glia-like cells that form the floor and walls of the third ventricle. The growth or retraction of tanycytic end-feet, which are in contact with the capillary fenestrations, controls the access of GnRH nerve terminals to the pituitary portal circulation [4]. Blood-borne GnRH then reaches the anterior pituitary, where it acts on pituitary gonadotropes to modulate the secretion of luteinizing hormone (LH) and follicle stimulating hormone (FSH) into the general circulation, which in turn promote gametogenesis and gonadal steroid synthesis by the testes and ovaries [5]. Interestingly, the absence of the traditional BBB in the median eminence, as in certain other circumventricular organs, not only allows peptide neurohormones such as GnRH to easily reach their target cells in the pituitary, it also allows circulating peripheral signals to enter the brain by passive diffusion from the portal capillaries or active transport by tanycytes. In the context of a viral infection, however, this adaptation, necessary for the maintenance of bodily homeostasis by allowing the exchange of information between the brain and the periphery, could instead represent a breach in the brain's defenses against pathogens.

Several studies to date have shown that male COVID-19 patients display lower circulating testosterone levels than their uninfected counterparts [6], an effect that can last several months after recovery from infection [7], and that lower testosterone levels are correlated with worse clinical outcomes [8,9]. Here using human COVID-19 patient blood samples and post mortem brains, mouse models of SARS-CoV-2 brain infection as well as human fetal tissues and cell lines, we investigated whether this hypogonadism in COVID-19 patients could be due to the infection of hypothalamic GnRH neurons rather than purely peripheral, as assumed so far.

Results

We retrospectively measured plasma testosterone and gonadotropin concentrations, which serve as surrogates for GnRH release, in a cohort of 60 male COVID-19 patients, 35-82 years old, hospitalized in the intensive care unit (ICU) of the Lille Medical University Hospital (CHU Lille). Among these, around half the patients, of all ages, showed normal or near-normal testosterone levels (Group 4) whereas half showed evidence of hypogonadism or decreased testicular function as defined by severely low total testosterone levels (< 0.9 ng/ml) during their first week in the ICU (Figure 1a). However, contrary to previous reports, only 4 of these 31 hypogonadal patients displayed the compensatory elevation of LH and FSH levels expected of individuals with a properly functioning hypothalamic-pituitary gonadal (HPG) axis (Group 3), whereas 16 showed intermediate LH levels of 2-12 IU/L (Group 2), and 11 presented clear hypogonadotropic hypogonadism, with LH levels below 2 IU/L (Group 1) (Figure 1b,c). COVID-19 patients who underwent an extended ICU stay were also sampled at weeks 2 and 4 in the ICU. In these, the functioning of the HPG was seen to switch between normal (Groups 3 and 4), i.e. where LH and testosterone were inversely correlated (log-linear model, $r^2 = 0.389$, $p = 1.88^{-11}$), and abnormal (Groups 1 and 2), i.e., where both LH and testosterone levels were low (Figure 1a-c). Among the 16 patients who died (26.6%), HPG axis function was abnormal in 12 (75%) at the time of death (Supplementary Figure 1a), whereas this condition was seen in only 11 out of 44 (25%) of the patients who survived (Supplementary Figure 1b) (mortality associated with abnormal HPG function, Pearson's Chi-squared $\chi^2_{(1)}$

= 10.38, p = 0.0013). Since obesity, which is characterized by resistance to elevated circulating levels of the adipocyte-derived metabolic hormone, leptin [10], is a known risk factor for severe COVID-19 [11], we also analyzed plasma leptin levels and body mass index (BMI) in these patients. While leptin was negatively correlated with testosterone levels, as expected [12] (Supplementary Figure 1c), neither BMI nor leptin levels appeared to be confounding factors for the phenotype (see Supplementary Table 1). Surprisingly however, given previous reports of a correlation between the intensity of the inflammatory response and low testosterone levels [13], the level of C-reactive protein (CRP), an indicator of inflammation, was also not found to be a confounding factor for hypogonadism (Supplementary figure 1d). Interestingly, COVID-19 patients with low LH/FSH levels (Groups 1 and 2) also displayed low levels of thyroid stimulating hormone, TSH (Supplementary figure 1e), whose releasing hormone, TRH, is secreted by hypothalamic neuroendocrine terminals in the median eminence similarly to GnRH [14,15]. Together, these results suggest that the severely low total testosterone levels seen in the majority of COVID-19 patients in intensive care are not just a reflection of gonadal insufficiency but of impaired hypothalamic function, or hypogonadotropic hypogonadism.

A central impairment of the HPG axis could result from either an absence of mature GnRH neurons or deficient/abnormal GnRH release [16]. Unlike other hypothalamic neurons driving bodily functions, GnRH neurons are not born in the brain but originate in the olfactory placode and migrate from the nose to the brain during embryogenesis [17,18], remaining in contact with the olfactory bulb (OB) via long dendrites [2]. Among the molecular cues key to GnRH neuronal development and function are the class 3 semaphorins, ligands of Neuropilin 1 (NRP1), which GnRH neurons themselves also express [19–22]. Together with angiotensin-converting enzyme 2 (ACE2), the known cell-surface receptor for SARS-CoV-2, and several proteases, including notably transmembrane protease, serine 2 (TMPRSS2), that cleave and prime the SARS-CoV-2 spike protein (S-protein) [23], NRP1 is also suspected of enhancing SARS-CoV-2 viral entry into target cells [24,25]. In light of these facts, we then assessed whether GnRH neurons could themselves be susceptible to infection by SARS-CoV-2 by isolating these neurons from *GnRH::Gfp* mice with the aid of fluorescence-activated cell sorting and quantifying the above molecules using RT-PCR. Although transcripts for TMPRSS2 were undetectable in these neurons, they expressed both *Nrp1* as well as *Ace2* (Supplementary Figure 2a), suggesting that in species such as humans in which the virus binds to the native ACE2 (unlike wild-type mice, which are infected by other coronaviruses but not SARS-CoV-2), adult GnRH neurons could indeed be a target of SARS-CoV-2.

Next, in order to investigate potential routes of infection of GnRH neurons, we used K18-hACE2 mice, a widely studied mouse model of coronavirus brain infection in which human ACE2 (hACE2) is expressed under the control of the keratin 18 promoter [26]. We found that 7 days after intranasal infection of these mice with SARS-CoV-2, transcripts for the nucleocapsid or N-protein were detected throughout the brain by RT-PCR using a set of Food and Drug Administration (FDA)-approved primers used to diagnose COVID-19 patients (Figure 2a; Supplementary Figure 2b,c). In addition, RNAscope studies clearly revealed the presence of transcripts for the S-protein in mitral cells of the olfactory bulb (Figure 2b). Interestingly, at 7 days post-infection, viral transcripts were much more abundant in the hypothalamus than in the OB or the

cortex (Friedman's multiple comparison test followed by an uncorrected Dunn's post test) (Figure 2a; Supplementary Figure 2c). Immunofluorescence labeling for the S- and N-proteins of SARS-CoV-2 showed massive viral infection in the whole brain in 4 out of 6 mice and viral infection restricted to the hypothalamus in 2 mice, recapitulating the RT-PCR data obtained from the same animals (Figure 2c). Our observations strengthen the possibility of a hematogenic route of viral infection through hypothalamic circumventricular organs lacking a BBB, which we have also recently shown to be targeted by SARS-CoV-2 [27], in addition to the more commonly accepted olfactory route [28,29]. Notably, several GnRH neurons were indeed seen to contain viral proteins (Figure 2c). The fluorescent signal for viral markers was completely absent in the brain of mock-infected K18-hACE2 mice (Figure 2d), validating the specificity of our tools to detect SARS-CoV-2 infection.

Given the putative susceptibility of GnRH neurons to SARS-CoV-2 and the existence of at least two potential infection routes revealed by our mouse models above, we next asked whether these suppositions were borne out in COVID-19 patients. We looked for the presence of viral proteins and RNA in the brains of four patients who died of COVID-19, including one who displayed viremia at the time of death, and compared them with the brains of four age-matched uninfected patients (negative nasal swab PCR or deceased before the pandemic). All patients died in the ICU (Supplementary Table 1). Using the same 3 pairs of primers used to diagnose patients in the USA and used to detect viral infection in K18-hACE2 mouse brains above (Figure 2a), we observed that three of the four COVID-19 patients, including the one who had viremia at the time of death, had readily detectable levels of N-protein transcripts in the hypothalamus (Figure 3a). Next, we succeeded in performing multiplex fluorescent in situ hybridization (RNAscope) in the hypothalamus in human brain tissue fixed in paraformaldehyde for longer than a week, and detected S-protein transcripts in vessels, some neuron-like cells and cells of the ependymal wall, while such labeling was absent in control patients despite the strong visualization of positive-control U6 mRNA (Figure 3b).

Immunofluorescence labeling also revealed abundant N-protein and double-stranded RNA (dsRNA) in numerous cells of the median eminence/infundibular nucleus of COVID-19 patients (Figure 3c,d), unlike uninfected controls (Figure 3c), indicating robust SARS-CoV-2 entry and replication. However, while N-protein was often colocalized with tanycytic processes, dsRNA labeling was fainter in tanycytic cell bodies lining the ventricular wall than in the nuclei of non-tanycytic cells morphologically associated with vimentin-immunoreactive tanycytic processes (Figure 3c,d). Interestingly, immunolabeling for S-protein, which mediates host-cell entry [23], was extremely high in ACE2- and TMPRSS2-coexpressing tanycytic end-feet, which contact fenestrated capillaries at the external pial surface of the median eminence (Figure 3e,f) and where they are known to interact morphologically with GnRH and TRH axon terminals [3,14,15]. In addition, despite the extreme paucity of GnRH neurons and their scattered distribution in the hypothalamus, we identified NRP1- or ACE2-positive GnRH neurons (Figure 4a,b), including several positive for the viral S-protein, in all COVID-19 patient brains (Figure 4b). Unexpectedly, more than one-third of GnRH neurons in COVID-19 patient brains displayed a bloated or abnormal morphology rather than the typical fusiform morphology, suggesting that they were sick or dying, while the number of GnRH

neurons with an abnormal morphology was negligible in control brains (Figure 4c,d). In keeping with the view that GnRH neurons were being killed by SARS-CoV-2 infection, GnRH neurons in all infected patient brains, but none in control subjects, were immunoreactive for cleaved caspase-3, and a majority of these dying neurons also displayed an abnormal morphology (Figure 4c,e). Further supporting the putative death or dysfunction of GnRH neurons on a massive scale, RT-PCR analysis of the hypothalamus of four COVID-19 patient brains revealed an almost complete disappearance of GnRH transcripts as compared to five control brains, whereas NRP1, which is expressed by other cell populations in the hypothalamus, was not significantly affected (Figure 4f).

Considering that GnRH neurons, which migrate through the OB to the hypothalamus, continue to maintain dendritic contact with the former, we also examined this tissue as an alternative route of infection. While we did not detect any residual GnRH neurons in the OB, immunofluorescence labeling showed abundant S-protein expression along with ACE2 and TMPRSS2 in the olfactory nerve layer (ONL), where olfactory marker protein (OMP)-expressing axons from sensory neurons of the olfactory epithelium enter the OB (Supplementary Figure 3a-c), confirming other reports of the olfactory epithelium and OB as ports of infection [29,30]. In addition, viral dsRNA was present in numerous OB cells bordering the ONL and within the glomerular layer of COVID-19 patient brains (Supplementary Figure 3c), unlike controls (Supplementary Figure 3b), indicating robust SARS-CoV-2 entry and replication along this second route of infection.

The existence of an olfactory route combined with the vulnerability of GnRH neurons to SARS-CoV-2 also raises another specter: that of an infection of these neurons by vertical transmission from the mother during embryonic development, which could impinge on the establishment and function of the HPG axis postnatally. Indeed, the migration, maturation and correct adult function of GnRH neurons, which are born in the nose during embryonic life, may be important for other aspects of brain development, such as the regulation of metabolism [19,31]. We therefore analyzed the expression of SARS-CoV-2 vulnerability factors in the olfactory epithelium of 7-, 11- and 14-week-old human fetuses. We found abundant expression of ACE2 and TMPRSS2 in neurons in the olfactory epithelium as well as their TAG-1-immunoreactive axons, which extend into the OB (Supplementary Figure 4), adding to previous reports of ACE2 and TMPRSS2 expression in other cell populations of the olfactory epithelium [32]. Serendipitously, we noticed on exploring the fetal nasal epithelium that neurons composing the vomeronasal organ, which disappears in adults [33], also abundantly expressed ACE2 and TMPRSS2 (Figure 5a-e), firmly establishing the susceptibility to viral infection of the birthplace of GnRH neurons (Figure 5f,g) as well as the axonal tracts along which they migrate into the brain (Figure 5h). Both GnRH neurons and the axonal scaffold composed of the olfactory and vomeronasal nerves also abundantly expressed NRP1 (Figure 5h), as we have previously shown [20], potentially further favoring SARS-CoV-2 cell entry [24,25].

Intriguingly, one of the molecules found to be differentially expressed in the lungs of COVID-19 patients is the formyl peptide receptor, FPR2/FPRL1/ALX [34], a G protein-coupled receptor and homolog of the Fpr family of vomeronasal receptors in mice. While FPR2 and its mouse equivalent are not considered to act

as vomeronasal receptors [35,36], it is active both in the brain and in immune cells, and is best known for its proinflammatory or inflammation-resolving actions depending on the activating ligand and signaling pathway triggered [37]. It also binds a variety of viral peptides and regulates viral RNA replication [38–40]. In light of all these facts, we investigated the presence of FPR2 protein by immunolabeling in the fetal nasal epithelium. To our surprise, FPR2 was not only richly expressed by neurons of the olfactory and vomeronasal epithelia and their axonal tracts, which constitute the migratory scaffold of GnRH neurons, it was also expressed by several GnRH neurons themselves (Figure 6a,b). Given the implication of FPR2 in the binding and replication of other RNA viruses, we reexamined the brains of infected K18-hACE2 mice and human COVID-19 patient brains for the expression of FPR2 transcripts and proteins. Interestingly, *Fpr2*, whose expression in control animals was quite low, was highly induced in the brains of K18-hACE2 mice following 7 days of SARS-CoV-2 infection (Figure 6c), and Fpr2 immunolabeling showed a strong colocalization with the distribution of SARS-CoV-2 S-protein in infected mice (Figure 6d). Immunolabeling studies also revealed the presence of FPR2 protein in the ONL and various hypothalamic cells in human COVID-19 patient brains (Figure 6e,f), with a remarkable increase in its expression in COVID-19 patient OBs as compared to control brains, reminiscent of our observations in infected mice and suggestive of its known upregulation by other viral dsRNAs [41]. Together, these results provide a striking indication that the combination of ACE2, NRP1 and FPR2 expression in adult and fetal human GnRH neurons and the human olfactory and vomeronasal epithelia during development could render these structures particularly vulnerable to SARS-CoV-2 infection.

Finally, to verify that human fetal GnRH neurons can indeed be infected by SARS-CoV-2, we tested the ability of pseudotyped viral particles expressing the full-length SARS-CoV-2 S-protein and the ZsGreen reporter gene [42] to infect a human GnRH-expressing cell line isolated from the fetal vomeronasal organ, FNC-B4 [43]. Interestingly, cells differentiating into GnRH neurons expressed ACE2 as well as NRP1 protein, and ACE2, NRP1 and FPR2 mRNAs (Figure 7a,b). Flow cytometry experiments further confirmed that a fraction of these cells were infected by the pseudotyped virus particles and expressed green fluorescence 48h later ($p=0.0235$, two-tailed unpaired t-test) (Figure 7c,d), strongly suggesting that at least some GnRH neurons in human fetuses could indeed be infected by SARS-CoV-2 in case of vertical transmission from infected mothers (see for example [44,45]).

Discussion

To summarize, our work demonstrates that GnRH neurons both in adult humans and in fetuses express multiple susceptibility factors for SARS-CoV-2 and can be infected by the virus, with potentially devastating long-term effects on later fertility as well as essential cognitive and metabolic processes. Multiple routes of infection of GnRH neurons in COVID-19 patients are possible. While we have previously shown that brain endothelial cells are infected by SARS-CoV-2, suggesting a hematogenic route for viral entry across the BBB [27], our current findings also provide support for an olfactory route both in fetuses and in adults. In addition, blood-borne SARS-CoV-2 viral particles extravasating from fenestrated vessels of the pituitary portal blood system may also directly attack GnRH neuroendocrine terminals that dip into

the perivascular space of these vessels, or infect ACE2-, TMPRSS2- and possibly FPR2-expressing tanycytes, whose end-feet surround GnRH neuronal terminals. While an alteration of GnRH secretion due to the infection of either the neurons themselves or of tanycytes could cause transient hypogonadotropic hypogonadism, in the worst-case scenario, the death of GnRH neurons that we observed in this normally stable population and the dramatic decrease in GnRH transcripts in the hypothalamus of COVID-19 patient brains, may have long-lasting effects on fertility in patients who survive infection. In addition, since tanycytes also tightly control the release of other neurohormones such as TRH into the pituitary portal circulation [14,15], and the external zone of the median eminence also harbors the neurosecretory terminals of TRH neurons, the infection of tanycytes or these other neurons associated with them may durably impact other physiological processes, and lead to endocrine-triggered neurological or psychiatric disorders. For instance, depression is known to occur in at least 33% of patients diagnosed with COVID-19 [46] and in up to 80% of hospitalized COVID-19 patients [47]. Strengthening this idea, the group of COVID-19 patients with hypogonadotropic hypogonadism also showed impaired TSH levels in our study. In addition, SARS-CoV-2 viral infection was also visualized in the paraventricular nucleus of the hypothalamus, where TRH neuronal cell bodies are located (Supplementary Figure 5), providing further support for a hematogenic route of infection in addition to the olfactory one, and emphasizing the need for the long-term monitoring of hormone levels in COVID-19 survivors.

The present study was conducted using blood samples from patients hospitalized in the ICU with severe COVID-19. However, while ICU hospitalization is itself known to be correlated with a transient drop in testosterone levels in male patients [7–9], the fact that more than half of these COVID-19 patients clearly displayed hypogonadism of hypothalamic origin points to the viral infection and not merely the ICU hospitalization as the cause of this alteration. This is especially preoccupying considering the current global decline in human fertility, including in Europe (https://www.euro.who.int/__data/assets/pdf_file/0010/73954/EN63.pdf). Whether similar phenomena could occur in patients with less severe infection remains to be investigated, perhaps in patients with “long COVID” to begin with. In addition, as a significant proportion of COVID-19 patients display anosmia or dysosmia [48] and defects in GnRH neuronal function may also be associated with alterations in olfactory perception [16,19,49], it would be interesting to investigate the long-term consequences of SARS-CoV-2 infection on fertility in anosmic and normosmic COVID-19 patients. In this regard, mutations in NRP1, a molecule that can potentiate SARS-CoV-2 host cell infection [24,25], causes Kallmann syndrome in humans, associating hypogonadotropic hypogonadism with anosmia [22], suggesting that NRP1-expressing cells like GnRH neurons and their migratory scaffold (17) might be especial targets of the virus. GnRH is also involved in regulating normal energy metabolism (29) and age-related changes in cognitive function [50], raising the possibility that the death or long-term dysfunction of these neurons following their infection may lead to metabolic and cognitive disorders in addition to reproductive ones.

In addition to ACE2 and NRP1, already known to mediate the host-cell binding and internalization of SARS-CoV-2, we identified a novel endogenous viral target in the brain and nasal epithelia – FPR2. Intriguingly, FPR1, which shares a number of ligands with FPR2, though not always with the same effect,

binds a highly conserved sequence of the SARS S-protein C-terminal region that is involved in membrane fusion [51] and is also present in the SARS-CoV-2 S-protein (https://www.uniprot.org/uniprot/P0DTC2#sequences). Together with our observations regarding the dramatic upregulation of FPR2 in the OB of COVID-19 patients as well as the hypothalamus of infected K18-hACE2 mice, this suggests that FPR2 is not only involved in SARS-CoV-2 pathogenesis but could act as an alternative receptor or co-receptor for the virus in both the brain and potentially the lung and other tissues. Its presence in GnRH neurons and their migratory scaffold, along with ACE2 and NRP1, could thus represent a triple whammy for these neurons. Interestingly, the modulation of systemic aging by GnRH neurons appears to be mediated by its regulation of the NFκB pathway [50]. The fact that FPR2 is known to modulate inflammation through the same pathway [52], and that moreover, the SARS-CoV-2 main protease, Mpro, cleaves NEMO, an essential modulator of NFκB that also plays a role in the survival of certain cells [27], suggests that the presence of FPR2 in GnRH neurons and its eventual upregulation by the virus may have far-reaching implications for neuroinflammation and neurodegeneration [36]. In addition, the unexpected expression of FPR2 in human fetal olfactory and vomeronasal tissues is intriguing leading one to question the traditional view that it is a uniquely “immune/inflammatory” FPR rather than a pheromone receptor in humans [35,36].

In light of the unusual vulnerability of fetal GnRH neurons, particular attention must also be paid to the consequences of maternal or perinatal COVID-19 infection in neonates [53], since the first postnatal activation of the HPG axis, i.e., minipuberty, a phenomenon that plays a key role in the later maturation of the reproductive system [54,55] and likely also in brain development in a broader sense, occurs during the infantile period. The impairment of minipuberty [56,57], for example by premature birth [58,59], may be correlated with the incidence of a range of non-communicable diseases or metabolic dysfunction later in life [58,59]. Studies following cohorts of babies born during the pandemic, and possibly treatments aimed at normalizing GnRH secretion, are therefore essential from a public health point of view to avoid a second pandemic of such diseases in the decades to come.

Methods

Ethics authorizations

All human tissues were obtained in accordance with French laws (Good Practice Concerning the Conservation, Transformation, and Transportation of Human Tissue to Be Used Therapeutically, published on December 29, 1998).

Adult COVID-19 patient brains and blood samples and control brains were obtained under authorization for the GonadoCOVID study (French protocol # 2-20-056 id8504) and authorized by the Lille Neurobiobank.

The studies on human fetal tissue were approved by the French agency for biomedical research (Agence de la Biomédecine, Saint-Denis la Plaine, France, protocol no.: PFS16-002). Non-pathological human

fetuses were obtained at GW7, GW11 and GW14 from voluntarily terminated pregnancies after written informed consent from the donors (Gynecology Department, Jeanne de Flandre Hospital, Lille, France).

Animal studies were performed with the approval of the Institutional Ethics Committees and the French Ministry of National Education, Higher Education and Research (APAFIS#2617-2015110517317420 v5, APAFIS#25384- 2020041515287655 v6).

COVID-19 ICU patient blood sample and hormonal analysis

Sixty male patients, 35-82 years of age, admitted to the resuscitation unit of the Lille University Hospital with a positive COVID-19 PCR were included in the “GonadoCOVID” study (French protocol # 2-20-056 id8504). Exclusion factors were a previous history of cancer or cirrhosis. Due to the difficulty of following the menstrual cycles of female patients in the ICU, female patients were excluded. For each patient, blood samples yielding 2000 µl of serum were obtained during the first week following admission, at 2 weeks and at 4 weeks if still hospitalized. The sampling week was defined based on the day the samples were obtained, where D1, D3, D5 sampling days were grouped to Week 1; J7, J9, J14 to week 2 and J30 to week 4. Sixteen patients died while in the ICU. Patient profiles are provided in Supplementary Table 1.

The patients were categorized into four groups based on the severity of the decrease in testosterone (T) and LH levels (Group 1: T <= 0.92 ng/ml & LH <=2 IU/L, Group 2: T < 0.92 ng/ml & LH > 2 & LH < 12 IU/L), Group 3: T < 0.92 ng/ml & LH > 12 IU/L, Group 4: T > 0.92 ng/ml). Unpaired t-tests were used to estimate the significance between the groups in terms of testosterone, LH, FSH and TSH levels using GraphPad Prism 8.

Pearson’s product moment correlation of (cor.test() of R stats version 4.0.3) was used to estimate the strength of linear association between leptin vs. testosterone as well as testosterone vs CRP in all patients irrespective of sampling week, while the relation between LH and testosterone levels in patients with normal HPG axis function followed a log-linear model (formula = LH ~ log(T)) determined using lm () of R stats version 4.0.3. The correlation plots as well as the dot plots showing testosterone or CRP levels in alive and deceased patients (n = 16) were generated using ggplot2 version 3.3.5 in R.

COVID-19 patient and control brains

The brains of 4 subjects (3 males and 1 female) who died of COVID-19 infection in the Lille University Hospital and 5 control subjects (4 males and 1 female) who did not test positive for COVID-19, including 2 who died before the pandemic began, were used for this study. COVID-19 and control subjects were matched for age, sex and comorbidities as far as possible. Their clinical characteristics are summarized in **Table 1**.

In keeping with strict protocols regarding the treatment of SARS-CoV-2-infected human tissues, human brains were immersion-fixed in 10% formalin for 1 week at room temperature. The hypothalamus was then dissected out and immersion-fixed in 4% paraformaldehyde in PBS 0.1M, pH7.4, for an additional 48h at 4°C, cryoprotected in 30% sucrose for an additional week at 4°C, embedded in Tissue-Tek and frozen in liquid nitrogen at the crystallization temperature of isopentane.

Human fetuses

Non-pathological human fetuses (7, 11 and 14 gestational weeks (GW), n = 1 per developmental stage) were obtained from voluntarily terminated pregnancies after written informed consent was obtained from the parents (Gynecology Department, Jeanne de Flandre Hospital, Lille, France). Fetuses were fixed by immersion in 4% PFA at 4°C for 5 days. The tissues were then cryoprotected in PBS containing 30% sucrose at 4°C overnight, embedded in Tissue-Tek OCT compound (Sakura Finetek), frozen on dry ice, and stored at -80°C until sectioning. Frozen samples were cut serially at 20 mm intervals with a Leica CM 3050S cryostat (Leica Biosystems Nussloch GmbH) and immunolabeled, as described below.

K18-hACE2 mice and SARS-CoV-2 infection

Mice expressing human ACE2 (hACE2) under the control of the keratin 18 (K18 or cytokeratin) promoter on a C57BL/6 background (B6.Cg-Tg(K18-hACE2)2Prlmn/J) were purchased from the Jackson Laboratory. Mice were housed under pathogen-free conditions at 21-22°C in a 12h light/dark cycle. Access to food and water was provided ad libitum throughout the experiment.

The BetaCoV/France/IDF0372/2020 strain of SARS-CoV-2 was supplied by the French National Reference Center for Respiratory Viruses hosted by the Institut Pasteur (Paris, France). Viral infection experiments were carried out in a biosafety level 3 (BSL3) facility at the French National Veterinary School in Maisons-Alfort, following a protocol approved by the ANSES/EnvA/UPEC Ethics Committee (CE2A- 16) and authorized by the French ministry of Research under the number APAFIS#25384-2020041515287655 v6 in accordance with French and European regulations. Male 8- to 10-week-old transgenic mice were anesthetized by i.p. injection of ketamine (100 mg per kg body weight) and xylazine (10 mg per kg body weight) and intranasally infected with 50 µl of DMEM containing 5 × 103 TCID50 of SARS-CoV-2. For brain preparation, animals were euthanized by an i.p. injection of pentobarbital (140 mg/kg body weight) 7 days after infection. Brains were removed and immersion-fixed in 4% PFA in PBS at 4 °C overnight and transferred to a 30% sucrose solution the next day. On the following day, brains were frozen and stored at −80 °C.

FNC-B4 human embryonic GnRH neuronal cell line

FNC-B4 cells [60] were kept in culture in Coon's modified Ham's F12 medium complemented with 10% FBS at 37°C and 5% CO2 and medium was changed twice weekly. Cells were used for pseudovirus infection and gene expression analysis when they reached 70% confluency. Gene expression assays for GnRH, ACE2, NRP1 and FPR2 were carried out on uninfected cells by quantitative RT-PCR.

Pseudotyped viral particle infection of cultured FNC-B4 cells for flow cytometry and immunocytofluorescence

Pseudotyped viral particles used for the infection were constructed by Asis Palazon (CIS bioGUNE, Spain) according to the method detailed in Crawford et al., 2020 [42] using a five-plasmid system lentiviral backbone 10 (CMV promoter to express ZsGreen Fluorescent Protein), the SARS-CoV-2 spike protein, HDM-Hgpm2, pRC-CMV-Rev1b and HDM-tat1b. Cells infected with the viral particles emit green fluorescence due to the expression of ZsGreen, allowing their detection by flow cytometry. FNC-B4 cells were infected by treatment with 1.1 × 104 viral particles per mL in conditioned medium for 36 hours. Cells were then trypsinized, pelleted at 1000g for 5 minutes and resuspended in PBS for flow cytometry. Flow cytometry was performed using a CytoFLEX LX flow cytometer (Beckman Coulter). The gating strategy was based on measurements of green fluorescence by comparing cell suspensions from green fluorescent positive cells and negative cells. For each replicate, green positive events were counted from a total of 50 000 events..

For immunocytofluorescence, FNC-B4 cells were plated on cover glasses coated with 0.01% Poly-L-lysine at low confluency. Cells were fixed in 4% PFA for 15 minutes and stored at 4°C in PBS containing 0.05% sodium azide. Prior to primary antibody incubation, unspecific binding sites were blocked and cells permeabilized using an incubation solution (0.3%Triton, 0.3% BSA in PBS, pH 7.4) for an hour at room temperature. Cells were then incubated with the primary antibodies (table) in incubation solution overnight at 4°C. After three washes with PBS, cells were incubated with secondary antibodies (table) in incubation solution for an hour at room temperature. After three washes, cells were counterstained with DAPI and mounted in Mowiol.

FACS-based isolation of GnRH neurons from GnRH:GFP mice

FACS isolation of GnRH::GFP neurons has been conducted as elaborated elsewhere[54,55]. Briefly, the proptic region was microdissected and dissociated using a Papain Dissociation System (Worthington) to obtain single-cell suspension. FACS was performed using an ARIA SORP cell sorter cytometer and FACSDiva 8.0 software (BD Bioscience). Data were analyzed using the Kaluza 2.0 software (Beckman Coulter). The sort decision was based on measurements of EGFP fluorescence (excitation: 488 nm, 50 mW; detection: GFP bandpass 530/30 nm, autofluorescence bandpass 695/40 nm) by comparing cell suspensions from the preoptic region and from the cerebral cortex of *Gnrh::Egfp* animals.

RNA extraction and quantitative RT-PCR analyses

For cultured human FNC-B4 cells, total RNA extraction was performed with the E.Z.N.A. Total RNA Kit I (cat: R6834-02 ,Omega Bio-tek, Inc.) according to the manufacturer's instructions. For human brain samples, total RNA was extracted from two fixed unstained hypothalamic slides (18µm each) using the ReliaPrep FFPE Total RNA Miniprep System (cat: Z1002, Promega). For mouse brain samples, the appropriate regions of the whole brain were dissected out and RNA extracted as above. RNA samples were immediately quantified using a Nanodrop apparatus and stored at -80°C until the reverse transcription step. For gene expression analyses, total RNA samples were reverse transcribed using the High-capacity cDNA Reverse Transcription kit (Applied Biosystems ref 4368814). For fixed human brain samples, a linear preamplification step was performed using the TaqMan PreAmp Master Mix Kit protocol (Applied Biosystems ref 4488593). Real-time PCR was then carried out using TaqMan Universal Master Mix II (Applied Biosystems ref 4440049) on the Applied Biosystems 7900HT Fast Real-Time PCR System. The TaqMan probes used in this study are listed below:

Mouse	Mm00607939_s1	Actb	Beta actin
Mouse	Mm03928990_g1	Rn18s	18S ribosomal RNA
Mouse	Mm01159006_m1	Ace2	Angiotensin I converting enzyme (peptidyl-dipeptidase A) 2
Mouse	Mm00484464_s1	Fpr2	Formyl peptide receptor 2
Mouse	Mm01253208_m1	Nrp1	Neuropilin 1
Mouse	Mm00443687_m1	Tmprss2	Transmembrane protease, serine 2
Human	Hs00171272_m1	GNRH1	Gonadotropin-releasing hormone 1
Human	Hs00826128_m1	NRP1	Neuropilin 1
Human	Hs99999901_s1	RN18S	Eukaryotic 18S RNA

The 18S ribosomal RNA was used as the housekeeping transcript for normalization. SARS-CoV-2 N-protein expression was assessed using the CDC 2019-Novel Coronavirus Real-Time RT-PCR Diagnostic Panel, as described elsewhere [61,62]. All gene expression data were analyzed using the 2-ΔΔCt method.

RNAscope labeling

Expression of the SARS-Cov2 S-protein in post mortem brains was assessed using a RNAscope® Multiplex Fluorescent Reagent kit v2 Assay and the V-nCov2019-S probe, reference: 848561 (both from Advanced Cell Diagnostics Inc.). Briefly, 20-µm thick hypothalamic sections cut on a cryostat, slides washed twice for 10 min in Gibco® DPBS (ThermoFisher) and dry baked in a HybEZ™ II oven (Advanced Cell Diagnostics Inc.) at 60°C for 30 min. They were then immersion-fixed in 4% paraformaldehyde PBS

0.1M, pH7.4, prepared in DEPC-treated water, for 1h at 4°C and washed again twice for 10 min in Gibco® DPBS. Next, the sections were processed according to manufacturer's instructions (ethanol dehydration, RNAscope hydrogen peroxide treatment and target retrieval), incubated with RNAscope protease IV for 10 min at room temperature, and the signal revealed using the RNAscope multiplex fluorescent assay.

Immunohistochemistry and quantification for viral and host-cell markers in human and mouse tissues

Dissected, postfixed and cryoprotected blocks of adult human patient brains containing the hypothalamus or olfactory bulb were cut into 20µm sections and mounted. A citrate-buffer antigen retrieval step, 10mM Citrate in TBS-Triton 0.1% pH 6 for 30 min at 70°C, was performed on 20µm sections. After 3 washes of 5 minutes with TBS-Triton 0.1%, sections were blocked in incubation solution (10% normal donkey serum, 1mg/ml BSA in TBS-Triton 0.1% pH 7,4) for 1 hour. Blocking was followed with primary antibody incubation (see Antibody table) in incubation solution for 48h at 4°C. Primary antibodies were then rinsed out, before incubation in fluorophore-coupled secondary antibodies or, in case of amplified immunolabeling, biotinylated secondary antibodies for 1h in TBS-Triton 0.1% at room temperature. For classic immunohistochemistry, secondary antibodies were washed and sections counterstained with DAPI (D9542, Sigma). For amplified immunohistochemistry, after secondary antibodies were rinsed, sections were incubated with VECTASTAIN® Elite ABC-HRP kit (PK-6100, Vector laboratories) following manufacturer's instructions. Sections were then incubated with biotinyl-tyramide reagent (SAT700001EA, Perkin Elmer) following manufacturer's recommendations, washed and incubated with fluorophore-coupled streptavidin (1/500 dilution in TBS-Triton 0.1%) before counterstaining with DAPI. Finally, the sections were incubated with Autofluorescence Eliminator Reagent (2160, Millipore) following manufacturer's instructions and mounted with Fluoromount™ (F4680, Sigma). Immunolabeling in the human brain using the two antibodies to human ACE2 (R&D Systems, with tyramide amplification, and Abcam, without amplification), labeled similar cells.

For immunolabeling of human fetuses, 20 µm-thick sections of entire heads at GW 7, GW 11 and GW 14 were processed as follows. Slides first underwent antigen retrieval for 20 minutes in a 5mM citrate buffer heated to 90°C, then were rinsed in TBS and blocked/permeabilized for 2 hours at room temperature in TBS + 0.3% Triton + 0.25% BSA + 5% Normal Donkey Serum ("Incubation solution", ICS). Sections were then incubated with primary antibodies (see Antibody table) for two nights at 4°C in ICS. After rinses in TBS, the sections were incubated with secondary antibodies for two hours at RT in ICS, then rinsed again in TBS. Finally, nuclei were stained with DAPI (Sigma D9542, 1:5000 in TBS) for 5 minutes, and sections were rinsed before coverslipping with homemade Mowiol.

For immunolabeling of mouse brain sections, 30 µm-thick floating sections were rinsed 4 times in 0.1 M PBS pH 7.4 and blocked for 1 hour at room temperature in blocking solution (PBS containing 10% normal donkey serum and 0.3% Triton X-100). Sections were incubated overnight at 4°C with a mix of primary antibodies diluted in blocking solution (see Antibody table). The sections were washed three times in 0.1M PBS and incubated at room temperature for 1 hour with Alexa Fluor-conjugated secondary

antibodies (1:500 dilution; all purchased from Molecular Probes, Invitrogen, San Diego, CA) in blocking solution. A biotin-streptavidin amplification step was added for TMPRSS2 to verify expression in some tissues. The sections were then rinsed 3 times in 0.1 M PBS. Nuclei were counterstained by incubating the sections for 1 minute in DAPI before mounting and coverslipping as above.

Antibodies for immunohistochemistry

Antibody	*Manufacturer*	*Reference*	*Dilution*	*Tissue on which used*
Goat anti human ACE2	R&D Systems	AF933	1/100	Human
Rabbit anti human ACE2	Abcam	Ab15348	1/100-1/200	Human
Rabbit anti-TMPRSS2	Abcam	Ab92323	1/100-1/1000	Human
Mouse anti-FPR2	Invitrogen	GM1D6	1/100-1/400	Mouse & Human
Chicken anti-vimentin	Millipore	AB5733	1/500	Human
Goat anti-TAG1	R&D Systems	AF4439	1/500	Human
Goat anti-OMP	Wako	544-10001	1/200	Human
Guinea Pig anti GnRH	Erik Hrabovszky		1/3000-1/6000	Human, Mouse, Cells
Mouse anti-dsRNA	SCICONS J2	1001050	1/500	Mouse & Human
Mouse anti-SARS-CoV-2 spike protein	GeneTex	GTX632604	1/200	Human
Rabbit anti-SARS-CoV-2 spike protein	Sino Biological	40150-T62-Cov2	1/200	Mouse
Rabbit anti-SARS nucleocapsid protein	Novus Bio	NB100-56576	1/100	Mouse & Human
Goat anti-NRP1	R&D Systems	AF566	1/100	Human & Cells
Rabbit anti-cleaved caspase 3	Cell Signalling	#9664	1/200	Human

Statistics

Statistical comparisons were carried out using GraphPad Prism 8. All correlations were performed using *R stats version 4.0.3*.

Testosterone, LH, FSH and TSH levels were compared between the four COVID-19 patient groups (n=60 patients, 62 samples for Week 1) using an unpaired t-test.

For quantitative RT-PCR experiments (n=5 control patients vs. 4 SARS-CoV-2-infected patients; n=3 mock infected mice vs. 5 SARS-CoV-infected mice), a two-tailed unpaired t-test was used to compare expression levels between infected and control brains. The Friedman multiple comparison test followed by an uncorrected Dunn's post test was used to compare gene expression levels between the cortex, OB and hypothalamus of infected mice.

For the quantification of the proportion of GnRH neurons showing normal or abnormal morphology in control and COVID-19 patients, a two-way ANOVA was used, followed by Sidak's post hoc test (n=18 and 20 sections, 85 and 116 GnRH neurons, respectively; N=4 patients per group). To compare the proportion of GnRH neurons with normal or abnormal morphology that expressed cleaved caspase 3 in COVID-19 patients, a two-sided Fisher's exact test was used (n=66 GnRH neurons, N=4 patients).

Data from flow cytometry experiments were compared using an unpaired t-test.

Declarations

Author contributions

S.R. and V.P. designed the study, analyzed data, prepared the figures, and wrote the manuscript. F.S., S.N., D.F., CFFC. processed human and mouse tissues and performed immunofluorescence and multiplex in situ hybridization and qRT-PCR analyses, and all were involved in all aspects of study design, interpretation of results, and manuscript preparation; G.T., L.C., C.I.-G. and A.S. prepared tissues and performed immunofluorescence; K.C. performed FACS experiments. J.Dam, E.C. and R.J. performed the mouse infection experiments; A.P, J.E-O, M.M-G, produced the pseudotyped virus; E.H., F.T., contributed material, J.P., T.L. V.F., R.P., F.P. S.C.J., L.S., J.Dewisme and C.A.-M monitored patients and collected clinical samples and data; H.M.-F., V.F., M.B., M.M.-C., J.P., K.C., M.S., R.N., C.A.-M, P.P., V.M. and P.G. were involved in study design, interpretation of results, and preparation of the manuscript.

Acknowledgments

The authors are grateful to the LICORNE study group for access to patient brains. The Lille COVID Research Network acknowledges the contribution of residents, medical students, nursing teams, laboratory technicians and clinical research associates throughout the SARS-2-Cov pandemic.

Funding. This work was supported by European Research Council ERC-Synergy-Grant-2019-WATCH No 810331 (to R.N, V. P, and M.S.), ERC-2016-CoG-REPRODAMH No 725149 (to P.G.), ERC-2018-StG 804236-NEXTGEN-IO (to A.P), the European Union Horizon 2020 research and innovation program No 847941 miniNO (to K.C., V.P. and L.S.), DistAlz (no. ANR-11-LABEX-0009 to V.P. & F.P.), EGID (no. ANR-10-LABEX-0046 to V.P.), I-SITE ULNE (no. ANR-16-IDEX-0004) and benefited from the technical support of UMS2014-US41. The authors also acknowledge support of the INSERM Cross-Cutting Scientific Program (HuDeCA to P.G.), the ANR-3D Human (ANR-19-CE16-0021-02 to P.G.).

References

1. Seymen, C.M. The other side of COVID-19 pandemic: Effects on male fertility. *J Med Virol* **93**, 1396–1402 (2021).
2. Casoni, F., *et al.* Development of the neurons controlling fertility in humans: new insights from 3D imaging and transparent fetal brains. *Development* **143**, 3969–3981 (2016).
3. Baroncini, M., *et al.* Morphological evidence for direct interaction between gonadotrophin-releasing hormone neurones and astroglial cells in the human hypothalamus. *J.Neuroendocrinol.* **19**, 691–702 (2007).
4. Prevot, V., *et al.* The Versatile Tanycyte: A Hypothalamic Integrator of Reproduction and Energy Metabolism. *Endocr Rev* **39**, 333–368 (2018).
5. Clasadonte, J. & Prevot, V. The special relationship: glia-neuron interactions in the neuroendocrine hypothalamus. *Nat Rev Endocrinol* **14**, 25–44 (2018).
6. Salonia, A., *et al.* Severely low testosterone in males with COVID-19: A case-control study. *Andrology* **9**, 1043–1052 (2021).
7. Salonia, A., *et al.* Testosterone in males with COVID-19: A 7-month cohort study. *Andrology* (2021).
8. Dhindsa, S., *et al.* Association of Circulating Sex Hormones With Inflammation and Disease Severity in Patients With COVID-19. *JAMA Netw Open* **4**, e2111398 (2021).
9. Cinislioglu, A.E., *et al.* The relationship of serum testosterone levels with the clinical course and prognosis of COVID-19 disease in male patients: A prospective study. *Andrology* (2021).
10. Caro, J.F., *et al.* Decreased cerebrospinal-fluid/serum leptin ratio in obesity: a possible mechanism for leptin resistance. *Lancet* **348**, 159–161 (1996).
11. Simonnet, A., *et al.* High Prevalence of Obesity in Severe Acute Respiratory Syndrome Coronavirus-2 (SARS-CoV-2) Requiring Invasive Mechanical Ventilation. *Obesity (Silver Spring)* **28**, 1195–1199 (2020).
12. Luukkaa, V., *et al.* Inverse correlation between serum testosterone and leptin in men. *J Clin Endocrinol Metab* **83**, 3243–3246 (1998).

13. Lanser, L., *et al.* Testosterone Deficiency Is a Risk Factor for Severe COVID-19. *Front Endocrinol (Lausanne)* **12**, 694083 (2021).
14. Muller-Fielitz, H., *et al.* Tanycytes control the hormonal output of the hypothalamic-pituitary-thyroid axis. *Nat Commun* **8**, 484 (2017).
15. Farkas, E., *et al.* A Glial-Neuronal Circuit in the Median Eminence Regulates Thyrotropin-Releasing Hormone-Release via the Endocannabinoid System. *iScience* **23**, 100921 (2020).
16. Boehm, U., *et al.* Expert consensus document: European Consensus Statement on congenital hypogonadotropic hypogonadism--pathogenesis, diagnosis and treatment. *Nat Rev Endocrinol* **11**, 547–564 (2015).
17. Wray, S., Grant, P. & Gainer, H. Evidence that cells expressing luteinizing hormone-releasing hormone mRNA in the mouse are derived from progenitor cells in the olfactory placode. *Proc Natl Acad Sci U S A* **86**, 8132–8136 (1989).
18. Schwanzel-Fukuda, M. & Pfaff, D.W. Origin of luteinizing hormone-releasing hormone neurons. *Nature* **338**, 161–164 (1989).
19. Vanacker, C., *et al.* Neuropilin-1 expression in GnRH neurons regulates prepubertal weight gain and sexual attraction. *EMBO J* **39**, e104633 (2020).
20. Hanchate, N.K., *et al.* SEMA3A, a Gene Involved in Axonal Pathfinding, Is Mutated in Patients with Kallmann Syndrome. *PLoS Genet* **8**, e1002896 (2012).
21. Giacobini, P., *et al.* Brain Endothelial Cells Control Fertility through Ovarian-Steroid-Dependent Release of Semaphorin 3A *PLoS Biol* **12**, e1001808 (2014).
22. Marcos, S., *et al.* Defective signaling through plexin-A1 compromises the development of the peripheral olfactory system and neuroendocrine reproductive axis in mice. *Hum Mol Genet* **26**, 2006–2017 (2017).
23. Hoffmann, M., *et al.* SARS-CoV-2 Cell Entry Depends on ACE2 and TMPRSS2 and Is Blocked by a Clinically Proven Protease Inhibitor. *Cell* **181**, 271-280 e278 (2020).
24. Cantuti-Castelvetri, L., *et al.* Neuropilin-1 facilitates SARS-CoV-2 cell entry and infectivity. *Science* **370**, 856–860 (2020).
25. Daly, J.L., *et al.* Neuropilin-1 is a host factor for SARS-CoV-2 infection. *Science* **370**, 861–865 (2020).
26. Zheng, J., *et al.* COVID-19 treatments and pathogenesis including anosmia in K18-hACE2 mice. *Nature* **589**, 603–607 (2021).
27. Wenzel, J., *et al.* The SARS-CoV-2 main protease M(pro) causes microvascular brain pathology by cleaving NEMO in brain endothelial cells. *Nat Neurosci* **24**, 1522–1533 (2021).
28. Iadecola, C., Anrather, J. & Kamel, H. Effects of COVID-19 on the Nervous System. *Cell* (2020).
29. de Melo, G.D., *et al.* COVID-19-related anosmia is associated with viral persistence and inflammation in human olfactory epithelium and brain infection in hamsters. *Sci Transl Med* **13**(2021).
30. Meinhardt, J., *et al.* Olfactory transmucosal SARS-CoV-2 invasion as a port of central nervous system entry in individuals with COVID-19. *Nat Neurosci* **24**, 168–175 (2021).

31. Franssen, D., *et al.* AMP-activated protein kinase (AMPK) signaling in GnRH neurons links energy status and reproduction. *Metabolism* **115**, 154460 (2021).
32. Fodoulian, L., *et al.* SARS-CoV-2 Receptors and Entry Genes Are Expressed in the Human Olfactory Neuroepithelium and Brain. *iScience* **23**, 101839 (2020).
33. Frasnelli, J., Lundstrom, J.N., Boyle, J.A., Katsarkas, A. & Jones-Gotman, M. The vomeronasal organ is not involved in the perception of endogenous odors. *Hum Brain Mapp* **32**, 450–460 (2011).
34. Blanco-Melo, D., *et al.* Imbalanced Host Response to SARS-CoV-2 Drives Development of COVID-19. *Cell* **181**, 1036-1045 e1039 (2020).
35. Boillat, M., Carleton, A. & Rodriguez, I. From immune to olfactory expression: neofunctionalization of formyl peptide receptors. *Cell Tissue Res* **383**, 387–393 (2021).
36. Busch, L., Vieten, S., Brodel, S., Endres, K. & Bufe, B. Emerging contributions of formyl peptide receptors to neurodegenerative diseases. *Biol Chem* (2021).
37. He, H.Q. & Ye, R.D. The Formyl Peptide Receptors: Diversity of Ligands and Mechanism for Recognition. *Molecules* **22**(2017).
38. Weiss, E. & Kretschmer, D. Formyl-Peptide Receptors in Infection, Inflammation, and Cancer. *Trends Immunol* **39**, 815–829 (2018).
39. Krepel, S.A. & Wang, J.M. Chemotactic Ligands that Activate G-Protein-Coupled Formylpeptide Receptors. *Int J Mol Sci* **20**(2019).
40. Alessi, M.C., Cenac, N., Si-Tahar, M. & Riteau, B. FPR2: A Novel Promising Target for the Treatment of Influenza. *Front Microbiol* **8**, 1719 (2017).
41. Ampomah, P.B., Moraes, L.A., Lukman, H.M. & Lim, L.H.K. Formyl peptide receptor 2 is regulated by RNA mimics and viruses through an IFN-beta-STAT3-dependent pathway. *FASEB J* **32**, 1468–1478 (2018).
42. Crawford, K.H.D., *et al.* Protocol and Reagents for Pseudotyping Lentiviral Particles with SARS-CoV-2 Spike Protein for Neutralization Assays. *Viruses* **12**(2020).
43. Maggi, M., *et al.* Expression and biological effects of endothelin-1 in human gonadotropin-releasing hormone-secreting neurons. *J Clin Endocrinol Metab* **85**, 1658–1665 (2000).
44. Fenizia, C., *et al.* Analysis of SARS-CoV-2 vertical transmission during pregnancy. *Nat Commun* **11**, 5128 (2020).
45. Facchetti, F., *et al.* SARS-CoV2 vertical transmission with adverse effects on the newborn revealed through integrated immunohistochemical, electron microscopy and molecular analyses of Placenta. *EBioMedicine* **59**, 102951 (2020).
46. Taquet, M., Geddes, J.R., Husain, M., Luciano, S. & Harrison, P.J. 6-month neurological and psychiatric outcomes in 236 379 survivors of COVID-19: a retrospective cohort study using electronic health records. *Lancet Psychiatry* **8**, 416–427 (2021).
47. Chou, S.H., *et al.* Global Incidence of Neurological Manifestations Among Patients Hospitalized With COVID-19-A Report for the GCS-NeuroCOVID Consortium and the ENERGY Consortium. *JAMA Netw*

Open **4**, e2112131 (2021).

48. Lechien, J.R., *et al.* Olfactory and gustatory dysfunctions as a clinical presentation of mild-to-moderate forms of the coronavirus disease (COVID-19): a multicenter European study. *Eur Arch Otorhinolaryngol* (2020).
49. Hellier, V., *et al.* Female sexual behavior in mice is controlled by kisspeptin neurons. *Nat Commun* **9**, 400 (2018).
50. Zhang, G., *et al.* Hypothalamic programming of systemic ageing involving IKK-beta, NF-kappaB and GnRH. *Nature* **497**, 211–216 (2013).
51. Mills, J.S. Peptides derived from HIV-1, HIV-2, Ebola virus, SARS coronavirus and coronavirus 229E exhibit high affinity binding to the formyl peptide receptor. *Biochim Biophys Acta* **1762**, 693–703 (2006).
52. Cattaneo, F., Parisi, M. & Ammendola, R. Distinct signaling cascades elicited by different formyl peptide receptor 2 (FPR2) agonists. *Int J Mol Sci* **14**, 7193–7230 (2013).
53. Figueiredo CP, F.-D.F., da Poian AT, Clarke JR. SARS-CoV-2-associated cytokine storm during pregnancy as a possible risk factor for neuropsychiatric disorder development in post-pandemic infants. Neuropharmacology. **201**, 108841. doi: 108810.101016/j.neuropharm.102021.108841 (2021).
54. Messina, A., *et al.* A microRNA switch regulates the rise in hypothalamic GnRH production before puberty. *Nat Neurosci* **19**, 835–844 (2016).
55. Pellegrino, G., *et al.* GnRH neurons recruit astrocytes in infancy to facilitate network integration and sexual maturation. *Nat Neurosci*, 10.1038/s41593-41021-00960-z (2021).
56. Kuiri-Hanninen, T., *et al.* Postnatal developmental changes in the pituitary-ovarian axis in preterm and term infant girls. *J Clin Endocrinol Metab* **96**, 3432–3439 (2011).
57. Kuiri-Hanninen, T., *et al.* Increased activity of the hypothalamic-pituitary-testicular axis in infancy results in increased androgen action in premature boys. *J Clin Endocrinol Metab* **96**, 98–105 (2011).
58. D'Onofrio, B.M., *et al.* Preterm birth and mortality and morbidity: a population-based quasi-experimental study. *JAMA Psychiatry* **70**, 1231–1240 (2013).
59. Luu, T.M., Katz, S.L., Leeson, P., Thebaud, B. & Nuyt, A.M. Preterm birth: risk factor for early-onset chronic diseases. *CMAJ* **188**, 736–746 (2016).
60. Vannelli, G.B., *et al.* Neuroblast long-term cell cultures from human fetal olfactory epithelium respond to odors. *J.Neurosci.* **15**, 4382–4394 (1995).
61. Sekulic, M., *et al.* Molecular Detection of SARS-CoV-2 Infection in FFPE Samples and Histopathologic Findings in Fatal SARS-CoV-2 Cases. *Am J Clin Pathol* **154**, 190–200 (2020).
62. Rhoads, D.D., *et al.* Comparison of Abbott ID Now, DiaSorin Simplexa, and CDC FDA Emergency Use Authorization Methods for the Detection of SARS-CoV-2 from Nasopharyngeal and Nasal Swabs from Individuals Diagnosed with COVID-19. *J Clin Microbiol* **58**(2020).

Tables

	Group	Age	Sex	BMI	Delay between first positive PCR and death (days)	Delay between the first positive PCR and the first negative one (days)	Resuscitation unit stay duration (days)	Post-mortem delay (hours)	Cause of death	Associated cause of death	Comorbidities
Patient 1	Ctrl	69	M	31	NA	NA	27	21	Septic shock due to Fournier's gangrene	Supra and sub tentorial ischemic injuries	Peripheral arterial disease, chronic glaucoma
Patient 2	Ctrl	62	M	?	NA	NA	25	19	Septic shock due to **Candida** fungemia	Fournier's gangrene due to rectal adenocarcinoma, Mesencephalic injuries	Stroke, arterial hypertension, dyslipidemia
Patient 3	Ctrl	64	F	?	NA	NA	NA	27	Unknown, probably due to a hemorrhagic shock following a psoas hemorrhage	Subacute cholecystis ; Peritoneal, retroperitoneal and perineal extensive psoas hematoma	Arterial hypertension, atrial fibrillation, aortic infectious endocarditis
Patient 4	Ctrl	36	M	28	NA	NA	0.1	80	Massive left ventricular infarction, extended to the interventricular septum	Arthérosclerosis	Atherosclerosis
Patient 5	Ctrl	50	M	?	NA	NA	NA	16	Ischemic heart disease	NA	Epilepsy, dyslipidemia
Patient 6	COVID	63	M	30	39	29	40	45	Multi-organ failure	Lung parenchyma damage (>75%) requiring ECMO, multiple septic shock	Basedow's Disease
Patient 7	COVID	82	M	28	67	NA	0	96	Disturbance of vigilance	Meningeal hemorrhage	Sensory neuropathy of all limbs, atrial fibrillation with left atrial closure, arterial hypertension, cerebral amyloid angeitis ?
Patient 8	COVID	63	F	20	55	Positive at death	25	17	Septic shock in context of refractory hypoxia	Invasive pulmonary aspergillose, lung parenchyma damage (25-50%)	Granulomatosis with polyangiitis
Patient 9	COVID	59	M	30	74	73	46	24	Septic shock	Multiple hemorrhagic and ischemic brain injuries,diffuse meningeal hemorrhage, multiple lacunes in the basal ganglia	Arterial hypertension

Table 1. Clinical characteristics of control and COVID-19 patients whose post mortem brains were used in the study

Figures

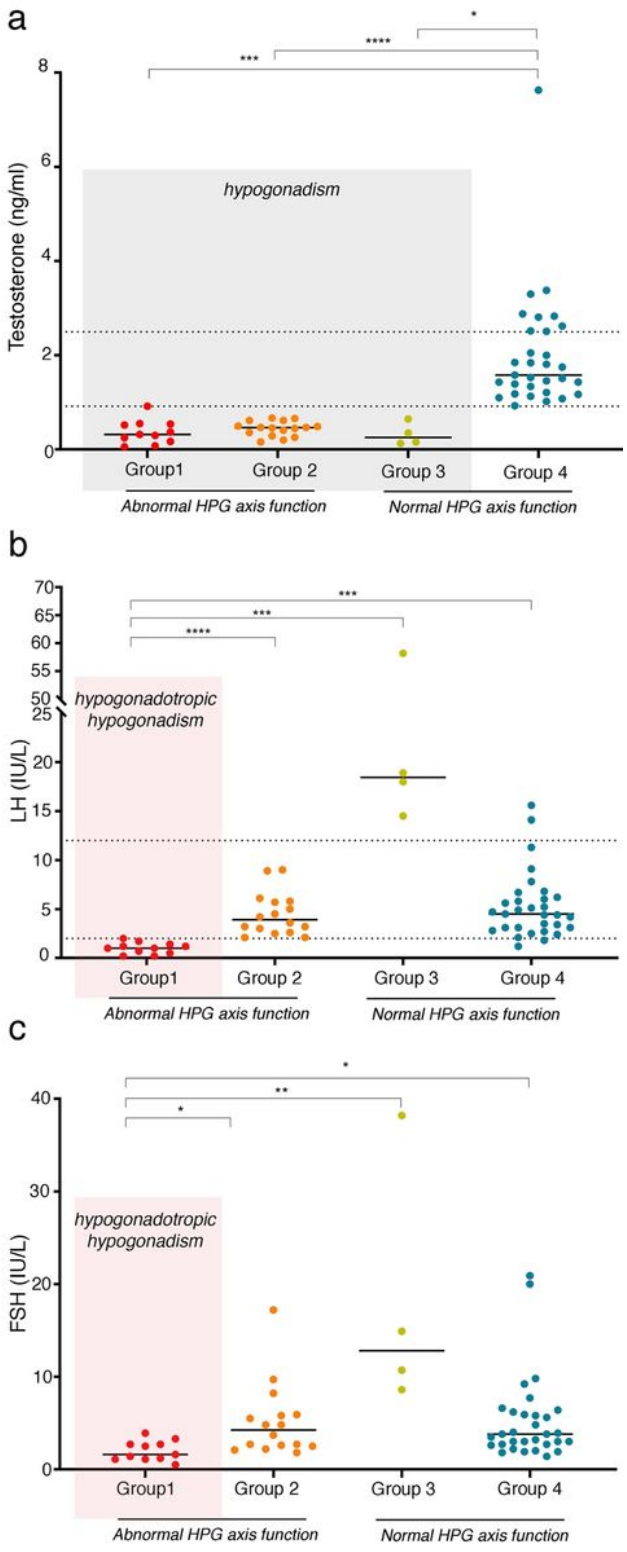

Figure 1

SARS-CoV-2 infection may cause hypogonadotropic hypogonadism in male COVID-19 patients. (a) Testosterone (two-tailed unpaired t-test, Group 4 vs Group 1, t(40) = 4.261, P = 0.0001; Group 4 vs Group 2, t(45) = 4.938, P < 0.0001; Group 4 vs Group 3, t(33) = 2.644, P = 0.0124 (b) luteinizing hormone (LH) (two-tailed unpaired t-test Group 2 vs Group 1, t(25) = 5.115, P < 0.0001; Group 3 vs Group 1, t(13) = 4.557, P = 0.0005; Group 4 vs Group 1, t(40) = 4.167, P = 0.0002, and (c) follicle stimulating hormone

(FSH) (two-tailed unpaired t-test, Group 2 vs Group 1, t(25) = 2.559, P = 0.0169; Group 3 vs Group 1, t(13) = 4.161, P = 0.0011; Group 4 vs Group 1, t(40) = 2.295, P = 0.0271) levels in COVID-19 patients, divided into 4 groups depending on whether total testosterone levels were severely decreased (hypogonadism; < 0.9 ng/ml) or not, and whether LH levels were appropriate (normal HPG axis function) or inappropriate (abnormal HPG axis function) for the observed testosterone level. A two-tailed unpaired t-test was used to estimate the significance of the difference between groups, where n=62 samples from 60 patients during first week of sampling (n for Group 1 = 11, Group 2 = 16, Group 3 = 4, Group 4 = 31) and *p < 0.05, **p < 0.01, ***p < 0.001, ****p < 0.0001, ns = non-significant.

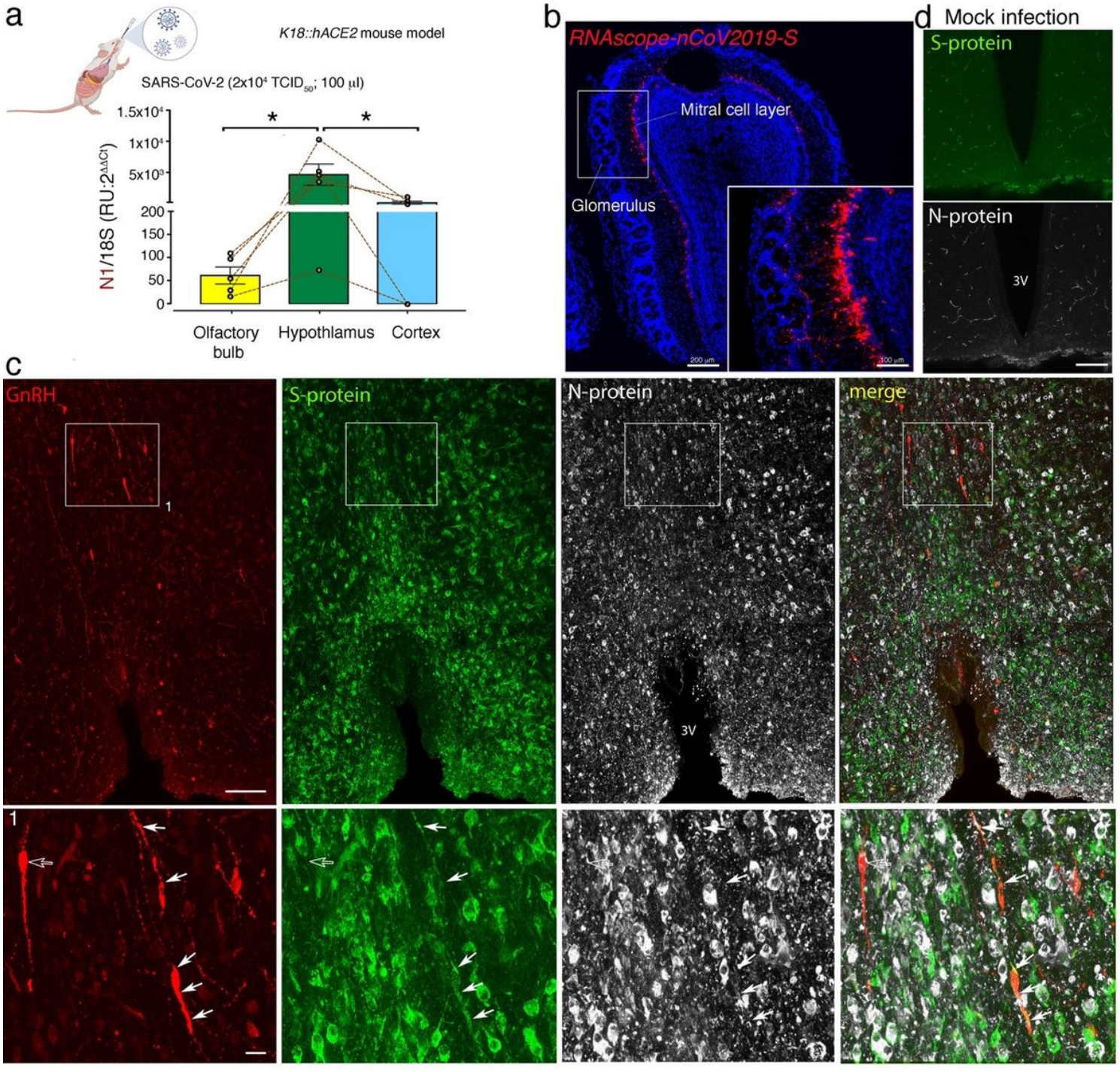

Figure 2

SARS-CoV2 infects GnRH neurons in the brain of the hACE2 mouse model. (a) Q-PCR analysis for N-protein transcript expression using the N1 probe in the olfactory bulb, hypothalamus and cortex 7d after K18::hACE2 mice were intranasally infected with SARS-Cov2 (results for the N2 and N3 are illustrated in Supplementary Figure 2b). Friedman's multiple comparison test (Fr=7,600, P= 0.0239) followed by an uncorrected Dunn's post test; Olfactory bulb vs. Hypothalamus P= 0.0114 and Cortex vs. Hypothalamus P= 0.0269. n=5 SARS-CoV-2-infected mice) (b) RNAscope labeling showing S-protein transcript expression (red) in the mitral cell layer of the olfactory bulb 7d after SARS-CoV2 infection. Blue: DAPI. Scale bar: 200 µm (Inset 200 µm). (c) Immunolabeling for GnRH (red), S-protein (green) and N-protein (white) in the preoptic region of the hypothalamus in K18::hACE2 mice 7d after SARS-CoV2 infection. 1: High magnification of the inset showing GnRH neurons expressing viral proteins (white arrow) or not (empty arrow). Scale bar: 200 µm (inset 20 µm). (d) Negative control showing the absence of immunolabeling for viral proteins in mock-infected mice. Scale bar: 200 µm.

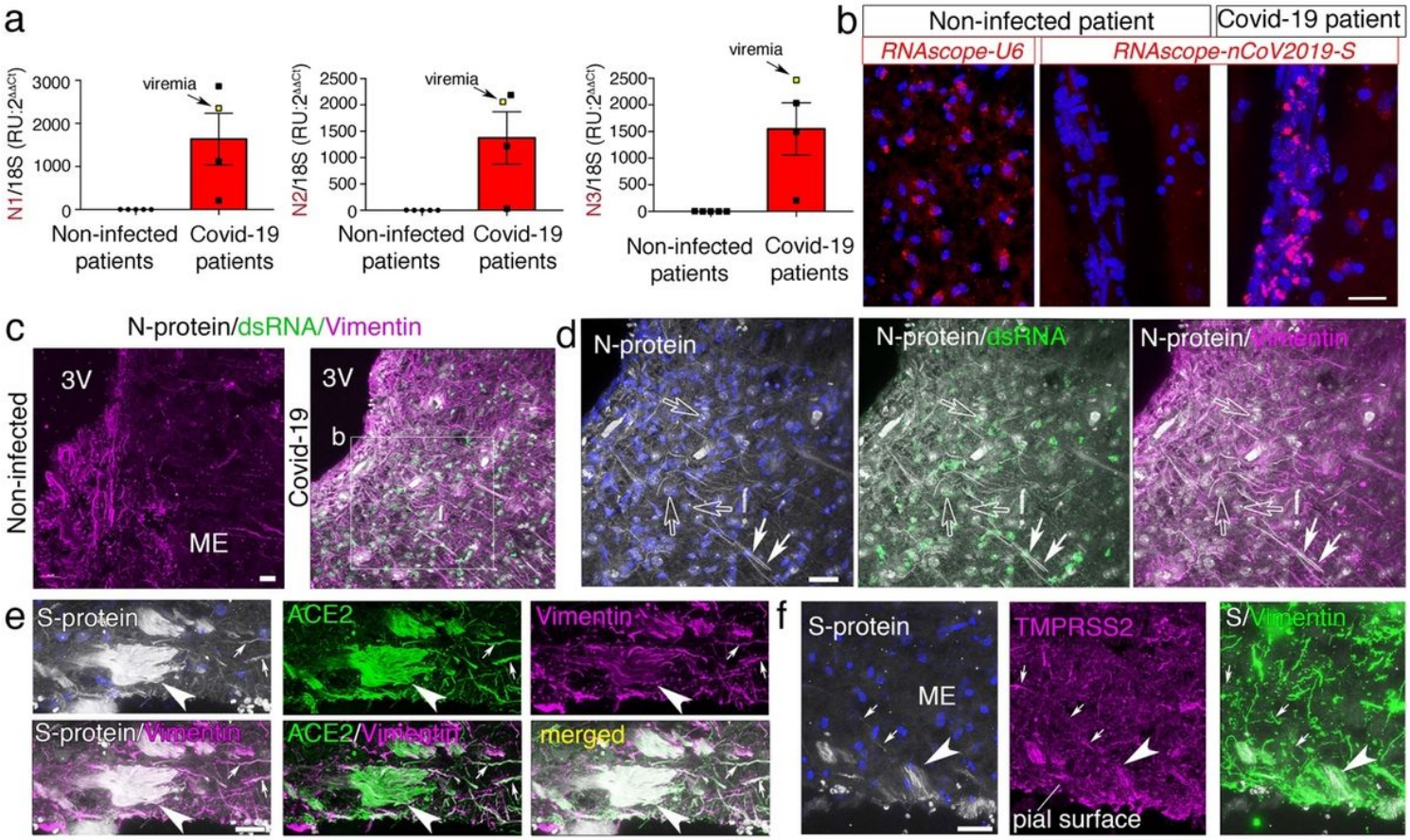

Figure 3

Expression of viral transcripts and proteins, ACE2 and TMPRSS2 in the hypothalamus of COVID-19 patients and non-infected controls. (a) Quantitative PCR analysis of N-protein mRNA in the hypothalamus of COVID-19 patients using three distinct sets of probes (N1, N2 and N3). n= 5 control patients and 4 SARS-CoV-2-infected patients. Note that one COVID-19 patient (yellow point) had viremia at the time of death. Two-tailed unpaired t test, for N1 t(7)=3.097, P= 0.0174, for N2 t(7)=3.143, P= 0.0163 and for N3 t(7)=3,587, P =0.0089). (b) RNAscope labeling for S-protein mRNA (pink) in the hypothalamus of a control

(non-infected) patient and a COVID-19 patient. U6 RNA was used as a positive control. Blue: DAPI. Scale bar: 20 μm. (c) Immunolabeling for SARS-CoV-2 N-protein (white), viral dsRNA (green) and vimentin (magenta) to identify tanycytes, indicating that viral markers are absent in the hypothalamus of controls (left) but heavily expressed in a 63-year-old COVID-19 patient (right). 3V: third ventricle. Scale bar: 30 μm. (d) N-protein (white), dsRNA (green) and vimentin (magenta) immunolabeling showing abundant N-protein colocalization with vimentin in numerous tanycytic fibers (white arrows) and its presence in non-tanycytic cell bodies (empty arrows) near the median eminence (ME). dsRNA is not present in the vimentin-rich tanycytic cell body layer lining the ventricular wall. Blue: DAPI. Scale bar: 30 μm. (e,f) Extremely strong labeling for S-protein (white) seen in the end-feet (white arrowhead) of tanycytes (vimentin; magenta in e; green in f), which also express ACE2 (green in e) and TMPRSS2 (magenta in f), at the pial surface of the ME, where tanycytic processes (white arrows) contact fenestrated capillaries. Blue: DAPI. Scale bar: 20 μm.

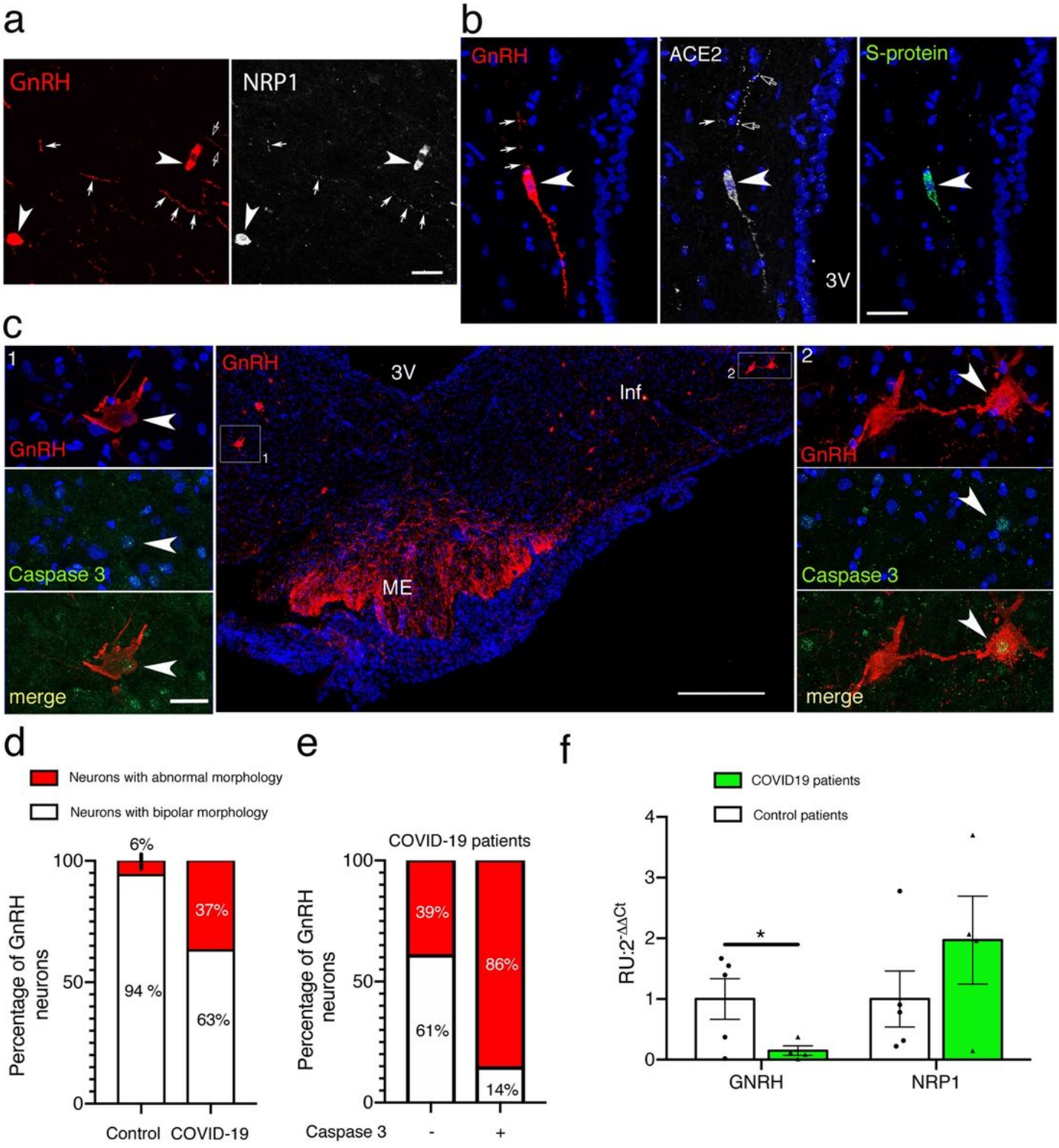

Figure 4

SARS-CoV-2 infects GnRH neurons and leads to their death in COVID-19 patients. (a) Immunolabeling for GnRH (red) and NRP1 (white) in hypothalamic GnRH neurons in a control patient. Arrowheads show a double-labeled GnRH neuron, while white arrows show a GnRH-immunoreactive process expressing NRP1. Scale bar: 50 µm. (b) Immunolabeling for GnRH (red), ACE2 (white), and S-protein (green) in hypothalamic GnRH neurons in a COVID-19 patient. Arrowheads show a triple-labeled GnRH neuron, white

arrows show a GnRH-immunoreactive process that does not express ACE2, and empty arrows show an ACE2-immunoreactive neuron-like process that does not express GnRH. Blue: DAPI. Scale bar: 50 μm. (c) Immunolabeling for GnRH (red) and cleaved caspase 3 (green) in the infundibular nucleus (Inf) - median eminence (ME) area of the hypothalamus of a COVID-19 patient. Blue: DAPI. Scale bars: 500 μm (inset 30 μm). (d) Quantification of proportion of GnRH neurons showing normal or abnormal morphology in control and COVID-19 patients (two-way ANOVA $F(2,108)=8.182$, $p=0.005$, followed by a Sidak's post hoc test, abnormal morphology in control vs. COVID-19 brains, $p=0.0016$, n=18 and 20 sections, 85 and 116 GnRH neurons, N=4 patients per group). (e) Proportion of GnRH neurons with normal or abnormal morphology expressing cleaved caspase 3 in COVID-19 patients (two-sided Fisher's exact test, $p=0.0387$, n=66 GnRH neurons, N=4 patients). (f) Quantitative RT-PCR for GnRH and NRP1 in the infundibular nucleus-median eminence of COVID-19 and control patients showing the almost complete disappearance of GnRH expression (Two-tailed unpaired t-test $t(7)=2.197$, $p=0.0320$ for control vs. COVID-19 brains. N=5 for control patient and N=4 for COVID-19 brains).

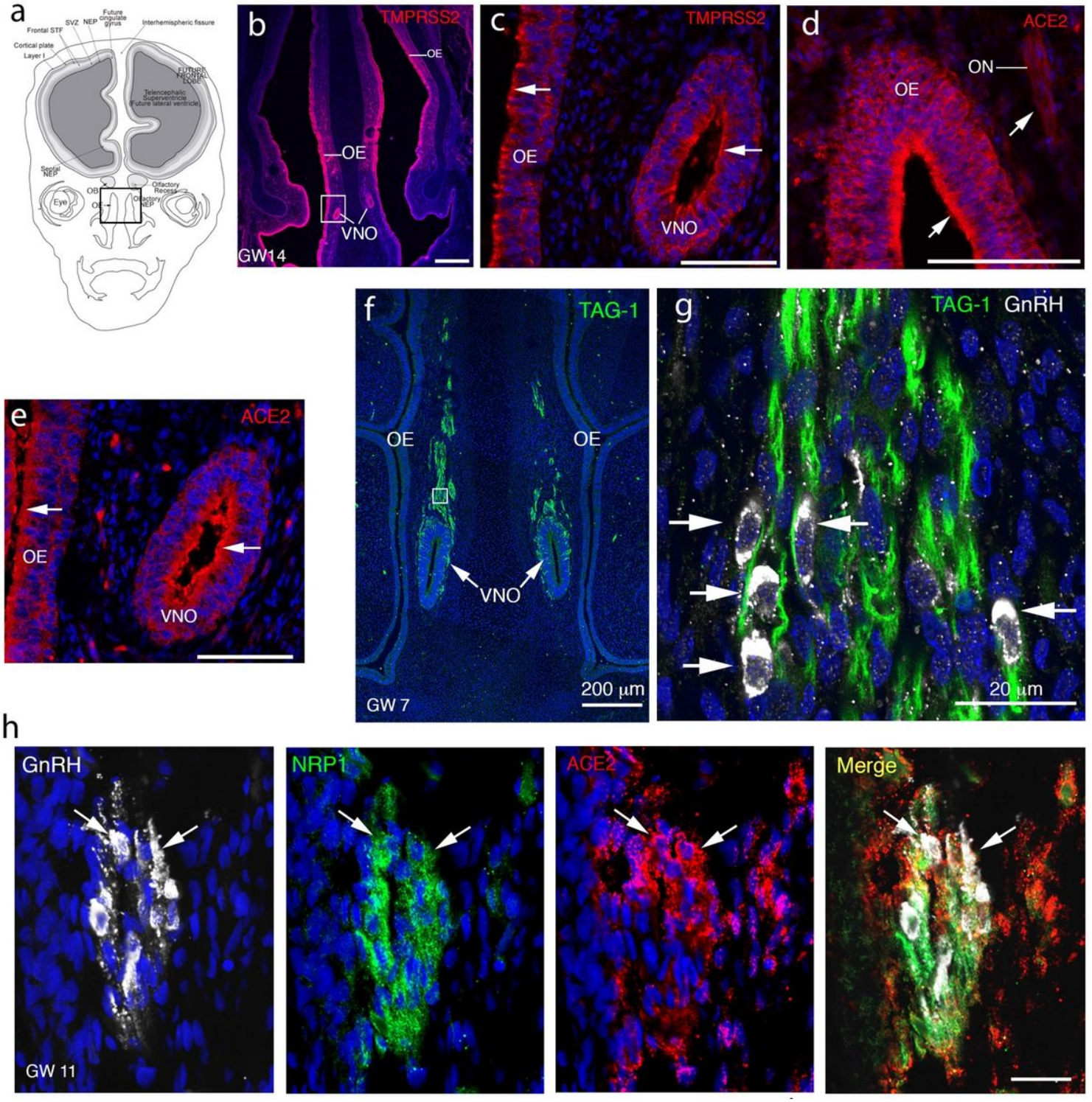

Figure 5

SARS-CoV-2 host susceptibility factors are expressed by human fetal olfactory and vomeronasal epithelia and newborn GnRH neurons (a) Schematic representation of a horizontal section through the nose and brain of a gestational week (GW) 14 human fetus, showing region immunolabeled in (b-e). (b-e) TMPRSS2 (c,d, red) and ACE2 (e,f, red) immunolabeling in the olfactory epithelium (OE), vomeronasal organ (VNO) and olfactory nerve (ON) of a GW 14 fetus. Blue: DAPI. Scale bars: 1 mm in b and 100 µm in c-e. (f,g) In a GW 7 human fetus, when GnRH neurons are born in the VNO, GnRH expression (white

arrows) begins as the neurons migrate out of the VNO along axon tracts of olfactory or vomeronasal sensory neurons labeled for TAG-1 (green) that are beginning to project to the presumptive olfactory bulbs. Blue: DAPI. Scale bar: 200 μm in f, 20 μm in g. (h) In a GW 11 human fetus, many GnRH neurons (white) migrating out of the VNO also express NRP1 (green) and/or ACE2 (red), host cell proteins that mediate SARS-CoV-2 infection (white arrows), while NRP1 and ACE2 are also expressed by some olfactory and vomeronasal nerve axons that form the scaffold for GnRH neurons. Blue: DAPI. Scale bar: 40 μm

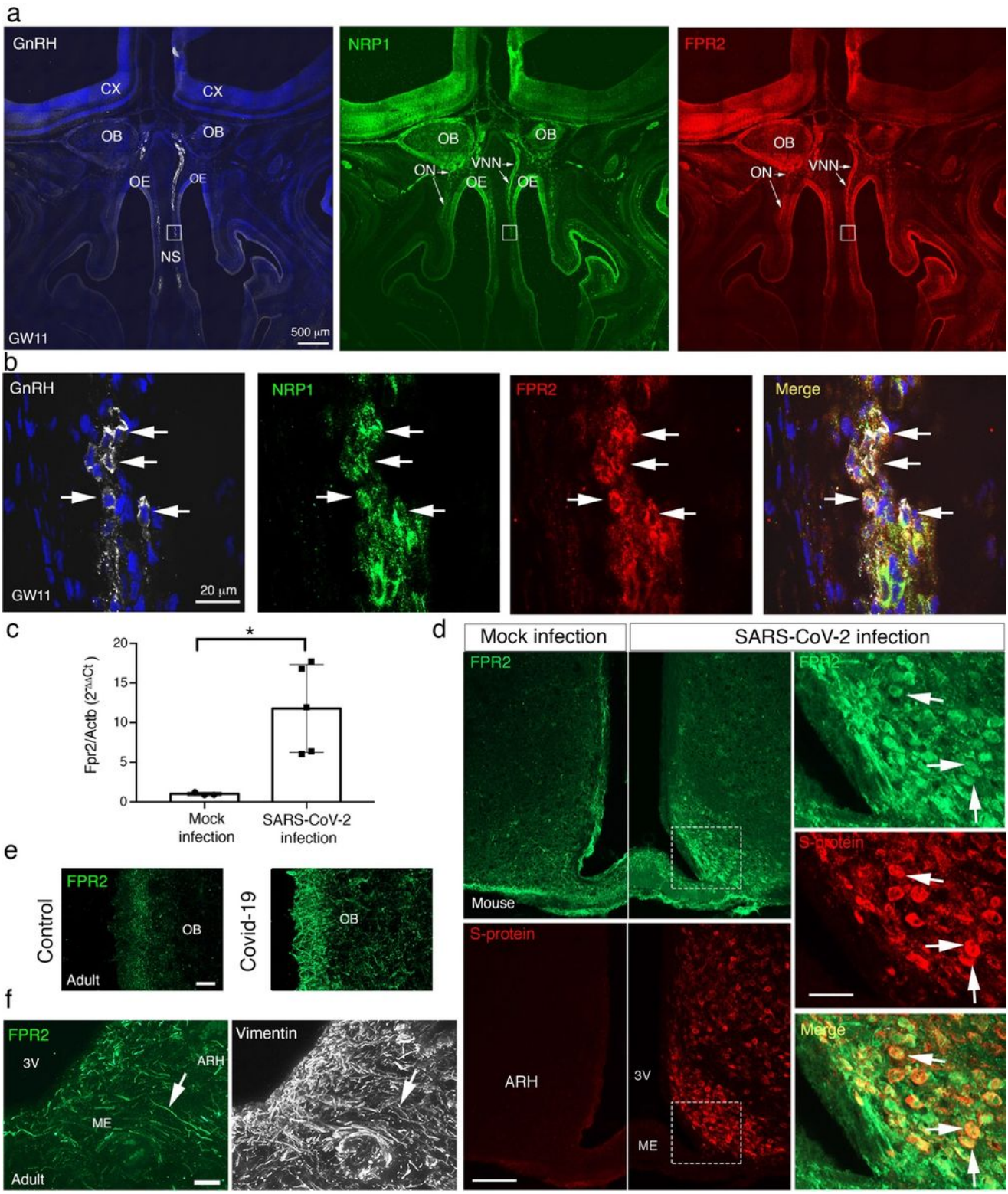

Figure 6

FPR2 is expressed by human fetal GnRH neurons and olfactory epithelium and is involved in SARS-CoV-2 pathogenesis in mice and humans. (a) Low-magnification images of immunolabeling for GnRH (white), NRP1 (green) and FPR2 (red) in a GW 11 human fetus, showing GnRH neurons migrating away from the vomeronasal (not shown) and olfactory epithelia (OE) along the vomeronasal nerves (VNN), towards the developing olfactory bulbs (OB) in the brain. Blue: DAPI. Olfactory nerve: on; nasal septum: ns. Scale bar: 500 µm. (b) High-magnification views of inset in (a) showing expression of NRP1 (green) and FPR2 (red) by newborn migrating GnRH neurons (white). Blue: DAPI. Scale bar: 20 µm. (c) Quantitative RT-PCR for Fpr2 expression relative to Actin B mRNA (Actb) in the hypothalamus of mock-infected and SARS-CoV-2-infected K18-hACE2 mice after 7d of infection (two-tailed unpaired t test t(6)=3.261, P= 0.0172, n= 3 mock and 5 SARS-CoV-2-infected mice). (d) Immunolabeling for FPR2 (green) and S-protein (red) in the median eminence (ME) / arcuate nucleus of the hypothalamus (ARH) region of K18-hACE2 mice 7d after mock or SARS-CoV-2¬¬ infection, showing high FPR2 expression in regions with high levels of infection, including many putative ARH neurons (white arrows). Third ventricle: 3V. Scale bars: 120 µm in low-magnification images, 60 µm in insets. (e) Increase in FPR2 immunolabeling (green) in the olfactory bulb (OB), in particular the olfactory nerve layer surrounding the OB, in a COVID-19 patient as compared to a control brain. Scale bar: 40 µm (f) Expression of FPR2 immunolabeling (green) in several cellular structures in the median eminence (ME) of a COVID-19 patient hypothalamus, including in vimentin-positive (white) tanycytic processes (white arrow). Third ventricle: 3V. Scale bar: 40 µm.

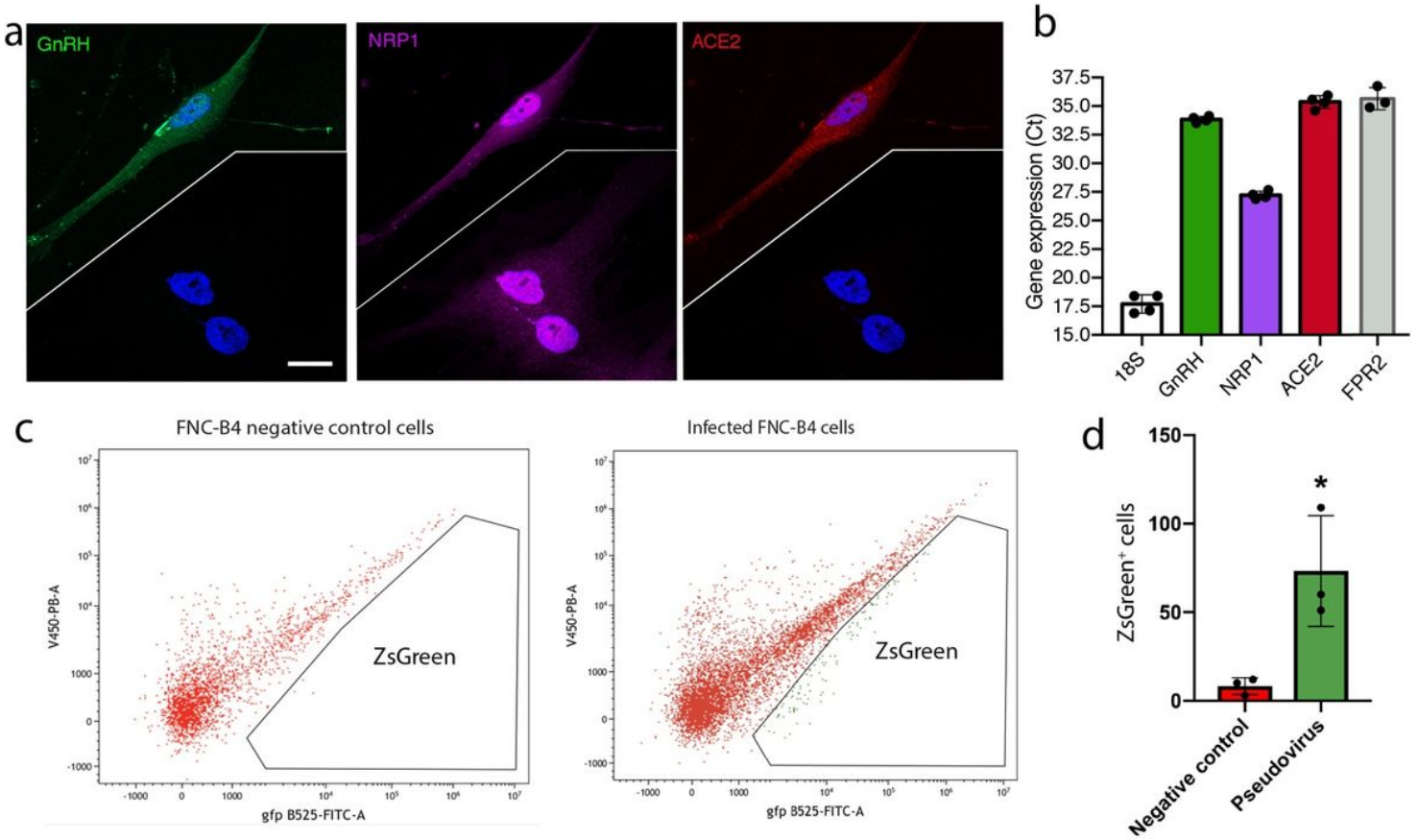

Figure 7

Susceptibility to SARS-CoV-2 viral or pseudoviral infection of a human fetal GnRH cell line, FNC-B4 (a) Differentiating FNC-B4 cells in culture showing the presence of NRP1 (magenta) and ACE2 protein expression (red) in cells that have begun to express GnRH (green, top view). Non-GnRH cells (bottom view) also express NRP1, in keeping with the more widespread expression of this guidance molecule in the fetal nose and brain. Blue: DAPI. Scale bar: 10 μm. (b) RT-PCR analysis demonstrating the expression of mRNAs for GnRH, NRP1, ACE2 and FPR2 by FNC-B4 cells. The housekeeping 18S RNA was used as a control. n=3 wells. (c) Fluorescence-activated cell sorting (FACS) of FNC-B4 cells (red) infected with pseudotyped lentiviral particles carrying a full-length SARS-CoV-2 spike protein and a ZsGreen reporter gene (green), showing infection of some cells by the pseudovirus. (d) ZsGreen expression, indicating pseudotyped viral particle entry, is almost undetectable in uninfected negative control cells treated only with vehicle (two-tailed unpaired t-test t(4)=3.566 p=0.0235, n=3 wells).

Supplementary Files

This is a list of supplementary files associated with this preprint. Click to download.

- SupplementaryFile.docx
- SupplementaryTable1.xlsx